PCCP

COMMUNICATION

View Article Online
View Journal | View Issue

Cite this: *Phys. Chem. Chem. Phys.*, 2025, **27**, 14733

Received 23rd March 2025,
Accepted 17th June 2025

DOI: 10.1039/d5cp01121c

rsc.li/pccp

Oxidation reduces spin-orbital coupling to achieve robust fluorescence emission in halogen-substituted dithieno[3,2-*b*:2′,3′-*d*]thiophene†

Huimin Liu,‡[a] Zeyan Zhuang,‡[c] Yawen Hou,[a] Yujiao Zhu,[a] Ruofeng Xu,[a] Bin Chen, *[a] Rong Hu *[b] and Zujin Zhao*[c]

The development of a reliable and feasible strategy for constructing organosulfur luminogens bearing good performance is highly desirable. Traditional organosulfur luminogens with large spin–orbit coupling (SOC) always possess weak emission both in solution and the solid state. Reducing SOC through an oxidation approach to obtain robust fluorescent luminogens has been rarely explored. In this study, we present dithieno[3,2-*b*:2′,3′-*d*]thiophene 4,4-dioxide (DTTO) and its halogen-substituted derivatives possessing robust deep blue fluorescence emission in THF and greenish emission in the solid state. Furthermore, the developed DTTO and its derivatives present aggregation-enhanced emission (AEE) behavior. Single-crystal analyses reveal that upon oxidation, multiple supramolecular interactions inhibit intramolecular motions of DTTOs in the solid state and enhance the fluorescence intensity. Additionally, density functional theory (DFT) calculations demonstrate that negligible SOC of DTTOs suppresses rapid intersystem crossing in the excited state and improves the radiative transition rate. For this initial discovery, oxidation reduces SOC to boost molecular fluorescence and provides a novel approach for developing luminescent organosulfur materials.

Introduction

Oxidation is a pervasive process in the universe, playing a crucial role in the Big Bang,[1] the evolution of matter,[2] aerobic respiration[3] and so on. This reaction typically incorporates oxygen atoms into reactants or results in the loss of electrons, leading to changes in valence states and molecular properties. For example, sulfuric acid, an important industrial raw material, is produced through the oxidation of sulfur ore. Additionally, sulfoxide and sulfone oxidized from the sulfur atom serve as functional groups in organic compounds and are widely utilized in medicinal and materials chemistry.[4–6] Furthermore, organosulfur compounds such as thiophene, thiazole, and their derivatives have garnered significant attention in the fields of organic light-emitting diodes (OLEDs),[7–9] organic solar cells,[10–12] and organic field-effect transistors (OFETs).[13–15] Commonly, organosulfur luminogens exhibit weak or even quenched emission in both solution and the solid state. This phenomenon is attributed to the lone-pair electrons of (n, π*) effect and intrinsic heavy atom effect on the sulfur atom.[16] These effects make molecules with large spin–orbit coupling (SOC) to facilitate rapid intersystem crossing.[17] Consequently, researchers have designed and synthesized molecules with large spin–orbit coupling to investigate applications in room-temperature phosphorescence,[18–20] quantum computing,[21–23] topological insulators,[24–26] and spintronics.[27–29] However, there is limited attention paid to reducing spin-orbital coupling in organic luminogens with heteroatoms and heavy atoms to obtain robust fluorescence emission. In order to challenge the conventional understanding of fluorescence quenching induced by heavy atom substitution in luminescent materials, we oxidized dithieno[3,2-*b*:2′,3′-*d*]thiophene (DTT)[30,31] and its halogen-substituted derivatives in dichloromethane (DCM) using m-CPBA. Following oxidation, dithieno[3,2-*b*:2′,3′-*d*]thiophene 4,4-dioxide (DTTO) displayed strong deep blue fluorescence in THF solution and greenish emission in the solid state. Moreover, DTTOs exhibit aggregation-enhanced emission (AEE) behaviors with varying THF/H_2O ratios. Furthermore, single crystal data reveal that DTTOs exhibit π–π and numerous weak interactions between adjacent molecules, which account for the AEE and fluorescence quenching behavior in the aggregated state. Theoretical investigations indicate that DTTs possess large SOC between the involved singlet and triplet states, which facilitates rapid

[a] *School of Material Science and Chemical Engineering, Ningbo University, Ningbo, Zhejiang, 315211, China*
[b] *School of Chemistry and Chemical Engineering, University of South China, Hengyang 421001, China*
[c] *State Key Laboratory of Luminescent Materials and Devices, Key Laboratory of Luminescence from Molecular Aggregates of Guangdong Province, South China University of Technology, Guangzhou, 510640, China*

† Electronic supplementary information (ESI) available. CCDC 2378911, 2378958, 2378965 and 2378966. See DOI: https://doi.org/10.1039/d5cp01121c

‡ These authors contributed equally to this work.

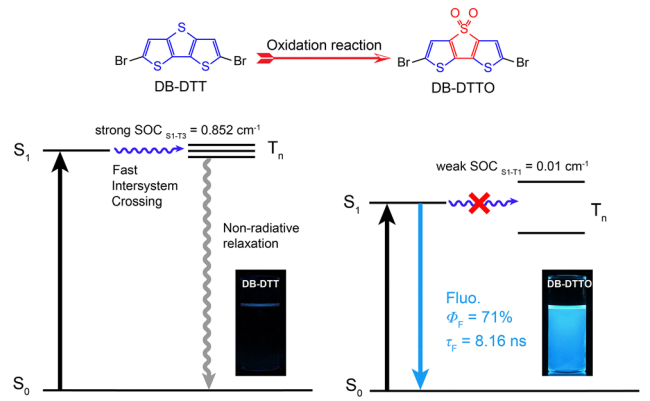

Fig. 1 Strategy to achieve excellent fluorescence emission by oxidation reaction. Representation of the excited-state decay pathways in DB-DTT and DB-DTTO in the solution state, respectively.

intersystem crossing and leads to non-radiative decay. In contrast, negligible SOC in DTTOs enhanced the radiative decay rate and exhibited excellent fluorescence emission. For this strategy, oxidation-reducing SOC in organosulfur molecules paves a new pathway to obtain robust luminogens for guiding molecular design (Fig. 1).

Results and discussion

Synthesis, characterization and photophysical properties

Herein, DTTO and its derivatives with different halogen-substitutions, namely DC-DTTO, DB-DTTO and DI-DTTO, were constructed through halogenation and oxidation of DTT. Fig. 2A illustrates the synthetic route and molecular structures of DTTs and DTTOs. The inset images show that DTTs hardly emit in the solid state under UV lamp irradiation, whereas the oxidized derivatives of DTTOs exhibit robust greenish fluorescence. The photophysical properties of the DTTOs are listed in Table 1. The detailed synthetic routes and characterizations are displayed in the ESI.† In order to investigate their photophysical properties, the UV-visible spectra of the DTTs and DTTOs in THF solution were measured, respectively. The absorption peaks of DTT are located at 282, 291, and 304 nm, indicating multiple electronic absorption transition states (Fig. 2B). This phenomenon should be attributed to electron vibronic transition in an excited state, like anthracene and pyrene.[32,33] Upon respective incorporation of chlorine, bromine, and iodine atoms at the α positions of DTT, the maximum absorption wavelengths of the derivative redshifted about 25 nm. This is attributed to the electron-donating conjugation effect of halogen atoms, which should increase the electron cloud density of DTT and reduce the absorption energy gap. Expectedly, upon oxidation, DTTO's absorption peak displayed a 47 nm redshift compared to that of DTT, and multiple absorption peaks disappeared. We propose that the sulfonyl group is a strong electron-withdrawing center and the adjacent thiophene ring is an electron donor; thus, strong intramolecular charge transfer results in a decreased energy gap. Due to the electron-donating conjugation effect, iodine atom substituted DI-DTTO among them has the maximum absorption peak at 384 nm with molar absorptivity of 1.37×10^4 L (mol^{-1} cm^{-1}). Meanwhile, chlorine or bromine-substituted DTTO have similar absorption peaks at 375 and 376 nm, respectively. For molecular states, as shown in Fig. 2C, DTT hardly emits in THF solvent, but DTTO exhibits robust deep blue fluorescence emission at 438 nm. Unexpectedly, halogen-substituted DTTOs also have excellent blue emission in solution as shown in Fig. S17 (ESI†). Furthermore, we investigated the photophysical behavior of DTTOs with varied THF/H_2O ratios (Fig. 2D). The emissive intensity of DI-DTTO gradually improves as the water content increases, and this is known as aggregation enhanced emission (AEE). However, beyond the water fraction of 80%, the fluorescence intensity suddenly decreases and the emissive wavelength redshifts 38 nm, which may be attributed to the solvent polarity increase and intermolecular strong π–π interactions. However, compared with erythrosin B, which is also a rigid structure with iodine atoms, it displays typical aggregation caused quenching (ACQ) in mixed THF/H_2O solutions as shown in Fig. S18 (ESI†). This demonstrates that rigid DI-DTTO has intriguing photophysical properties in the aggregated state. In contrast, the other three DTTOs have similar photophysical behaviors at different THF/H_2O ratios and the emissive intensity is hardly changed before 90% water fraction. In addition, the lifetimes and quantum yields of the DTTOs in THF are displayed in Fig. 2E and F. The lifetimes of the DTTOs were measured to be 9.59, 8.91, 8.16 and 2.69 ns, respectively, which determined that radiative transition was in the fluorescence range. Moreover, the planar rigid structures endow the DTTOs with high quantum yields of 58.9, 79, 71, and 34.8% respectively in the single molecular state. Thus, improving the emission intensity of DTTs through oxidation should be an efficient strategy.

Single-crystal structural analysis

To further elucidate the relationship between molecular structure and photophysical properties, single crystals of DTTOs grown from slow evaporation of DCM/hexane solution were investigated. According to ref. 34, rigid planar DTT stacks in a cofacial geometry with a π–π interaction distance of 3.938 Å. In contrast, DTTO also has a rigid configuration with two oxygen atoms incorporated on the central sulfur and a stacked cofacial geometry between adjacent molecules. Also, shorter π–π interaction distances (3.770 and 3.938 Å) exist, suggesting that DTTO has strong intramolecular charge transfer that increases the intermolecular dipole–dipole interaction (Fig. 3A). Surprisingly, halogen-substituted DTTO displayed parallel displaced stacking geometry. Regarding this, we proposed that halogens increase the electron cloud density on the thiophene ring, which results in improved electrostatic repulsion and parallel displacement happening. Moreover, the distances of π–π interaction become longer, especially in DI-DTTO (3.938, 3.946 and 4.183 Å) due to the iodine atom with maximum electron cloud density among them. Besides π–π interaction, Fig. 3E shows DI-DTTO with numerous supramolecular interactions among neighboring molecules, such as S═O···I, S═O···π, C–I···H,

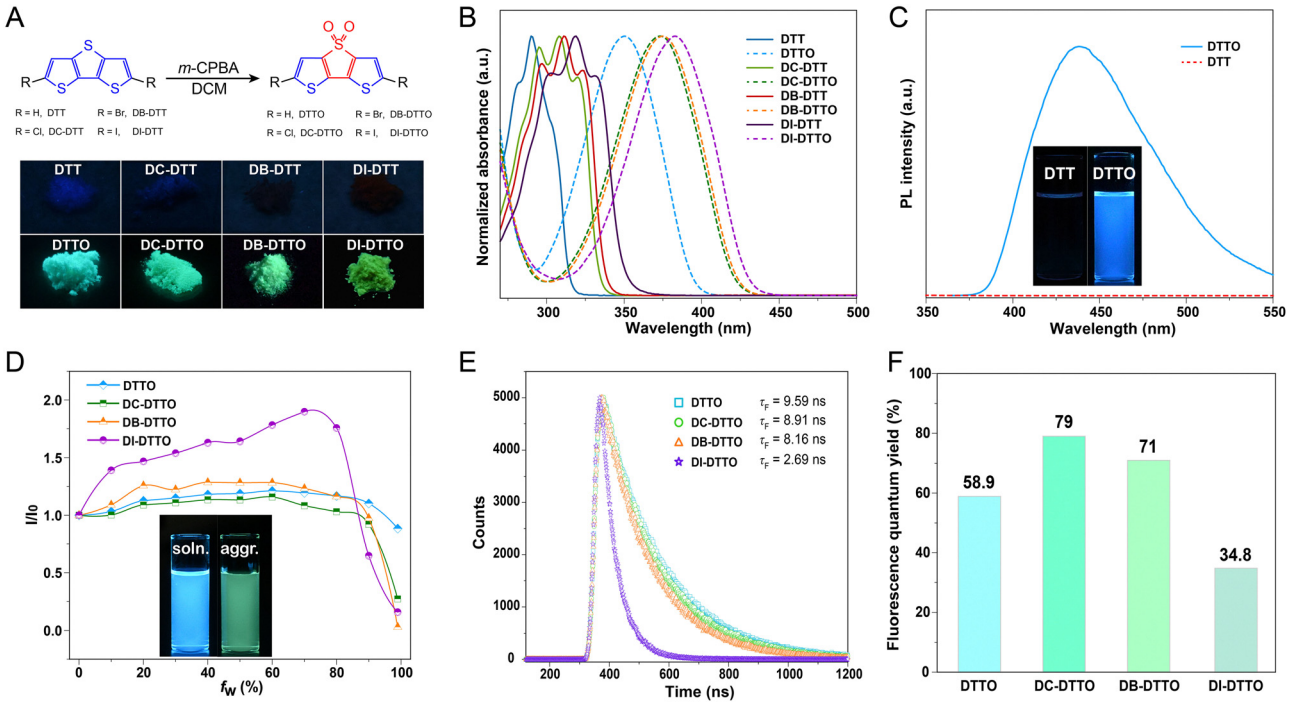

Fig. 2 (A) Synthetic route and molecular structures of DTTO with halogen substitution. (B) UV-vis spectra of DTTs and DTTOs. (C) PL spectra of DTT and DTTO in THF solution. (D) Plots between the ratio of I/I_0 and water fraction in H_2O/THF mixtures; I_0 and I are the maximum PL intensity of DTTOs in pure THF and in H_2O/THF mixtures (concentration: 1×10^{-5} mol L^{-1}), respectively; inset: fluorescence photograph of DI-DTTO in pure THF and in 99% H_2O/THF mixtures taken under 365 nm UV irradiation. (E) Fluorescence lifetimes, and (F) fluorescence quantum yields of DTTOs in THF solutions.

Table 1 Photophysical properties of DTTOs

Compound	λ_{abs}[a] (nm)	λ_{em} (nm)			τ[c] (ns)		Φ[d] (%)		ε ($\times 10^4$)
		Soln.[a]	Agg.[b]	Solid	Soln.[a]	Solid	Soln.[a]	Solid	
DTTO	351	438	480	494	9.59	7.19	58.9	12.7	0.94
DC-DTTO	375	468	483	491	8.91	6.67	79	41.5	0.76
DB-DTTO	376	469	489	495	8.16	1.12	71	3.7	0.74
DI-DTTO	384	467	505	510	2.69	0.82	34.8	0.7	1.37

[a] In THF solution (10^{-5} M), ε = molar absorptivity (L mol^{-1} cm^{-1}). [b] In 99% water fraction. [c] Fluorescence lifetime, measured at room temperature in air. [d] Fluorescence quantum yield, determined by a calibrated integrating sphere.

C–I···π, and S=O···S. We firmly believe that DI-DTTO actually has various stacking geometries in the aggregated state, such as edge to face, parallel displaced, parallel stacked and so on.[35–37] Thus, when DI-DTTO formed aggregates with water, numerous supramolecular interactions should inhibit molecular motions and improve the radiative transition. This can account for the pronounced AEE behavior of DI-DTTO before 80% water fraction. The fluorescence intensity dramatically decreased with water content further increasing; the strong π–π interactions between adjacent DI-DTTO in a confined space can result in emission quenching. For DTTO, DC-DTTO and DB-DTTO, they exhibit subtle AEE behavior due to less supramolecular interactions between neighboring molecules compared with DI-DTTO (Fig. 3B–D). The trade-off between molecular motion restriction and fluorescence quenching can happen with increased water, so the emission intensity of them changes slightly before 90% water fraction and suddenly quenches at 99%. The reason for their aggregate quenching at high water fraction should be similar to that for DI-DTTO.

Theory calculations

To deeply understand the photophysical properties of DTTs and DTTOs, we conducted theoretical calculations for further validation using the time-dependent density functional theory (TD-DFT) method. Fig. 4 displays that the highest occupied molecular orbital (HOMO) and the lowest unoccupied molecular orbital (LUMO) are primarily delocalized on the whole molecular skeleton of the DTTs and DTTOs. The energy gap between the LUMO and HOMO in the DTTs decreased with increased molecular weight of the halogen. This trend is consistent with experimental absorption variation due to the halogen's electron donating conjugation effect. As anticipated, DTT exhibits a relatively large spin–orbit coupling (SOC) of 0.595 cm^{-1} between S_1 and T_2, while SOC is generally below 0.1 cm^{-1} without heavy

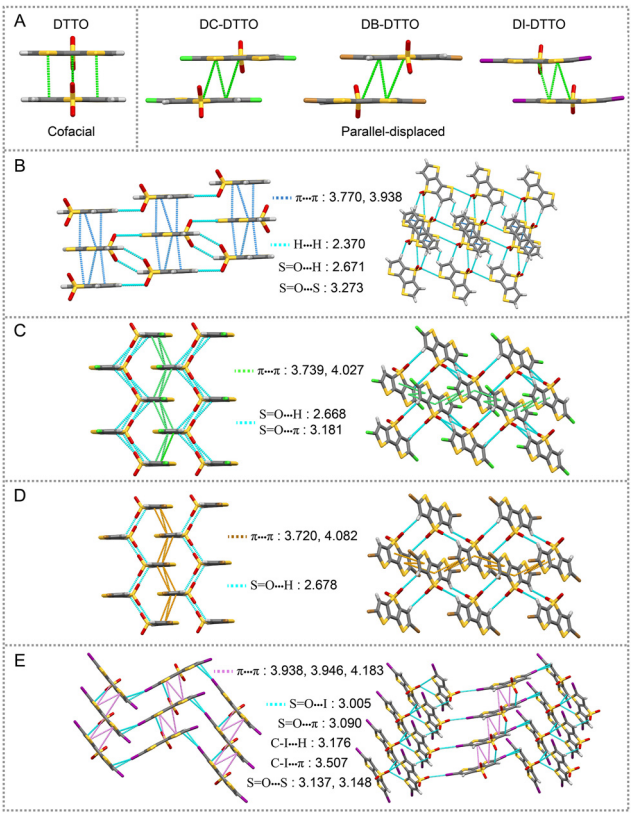

Fig. 3 (A) Adjacent molecular interaction geometries. Packing modes and intermolecular interaction distances of (B) DTTO, (C) DC-DTTO, (D) DB-DTTO and (E) DI-DTTO, respectively, in single-crystal X-ray diffraction analysis, unit: Å.

atoms.[38] With halogen substitution, the values of SOC further increased to 0.625, 0.852, and 1.896 cm^{-1}. As we know, the SOC is proportional to k_{ST} and the excited state can dissipate through rapid intersystem crossing (ISC) resulting in fluorescence quenching, which is known as the heavy atom effect. The heavy atom effect and π–π interactions synergistically decide the non-emissive behavior of DTTs in solution and the solid state. In contrast, the reduced energy gap between the LUMO and the HOMO of the DTTOs corresponds to a redshift in the UV-Vis spectra. Unexpectedly, due to the presence of heavy atoms in the DTTOs, they exhibit negligible SOC to suppress the rapid ISC process in the excited state. Thus, the enhanced radiative transition results in robust emission in the single molecular state. Due to the presence of heavy atoms, we proposed that the delocalized electron *via* them should facilitate spin and orbital coupling.[39] However, the strong electron-withdrawing sulfone center causes delocalized electron enrichment around it; the electrons *via* the heavy atom should become less and lead to negligible SOC. Thus, theoretical calculation explained the robust emission of DTTOs in dilute solution.

Fluorescence encoding

Based on the phenomenon of fluorescence activation following oxidation, we conducted a proof-of-concept study on fluorescence encoding and decoding using a 96-well plate, as illustrated in the schematic diagram in Fig. 5A. A solution of DC-DTT in DCM solvent was employed as the encoding precursor, which was added to the designated wells, while an equal volume of DCM was added to the remaining wells. Unsurprisingly, no information was visible under a UV lamp. Subsequently, a solution of m-CPBA in DCM was added to all wells, resulting in the turn on of the fluorescence under UV light immediately.

As shown in Fig. 5B, after writing information on the blank 96-well plate, no observable information was present under UV light. Upon the addition of the m-CPBA solution to each well, fluorescence appeared immediately, facilitating information reading. This method allows for the representation of letters such as "NB," numbers like "87," the Chinese character "回归," and the symbol for Sagittarius, demonstrating that information input and reading can be achieved through a pixel-like design. Furthermore, we can define the fluorescent-

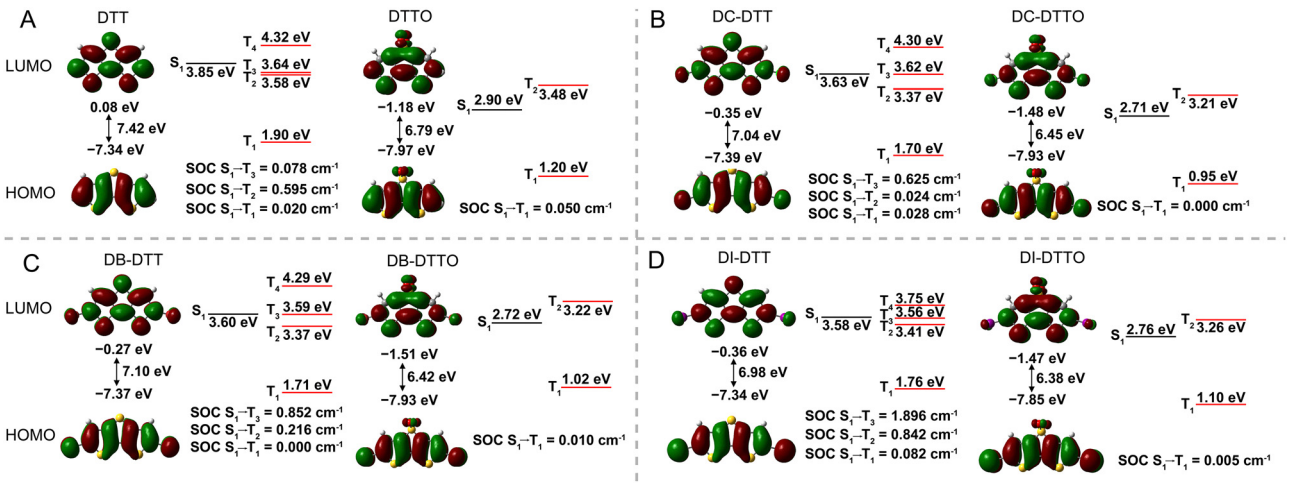

Fig. 4 Frontier molecular orbitals, adiabatic excitation energies for S_1 and T_n ($n \geq 1$) states, and associated SOC matrix elements of (A) DTT and DTTO, (B) DC-DTT and DC-DTTO, (C) DB-DTT and DB-DTTO, (D) DI-DTT and DI-DTTO.

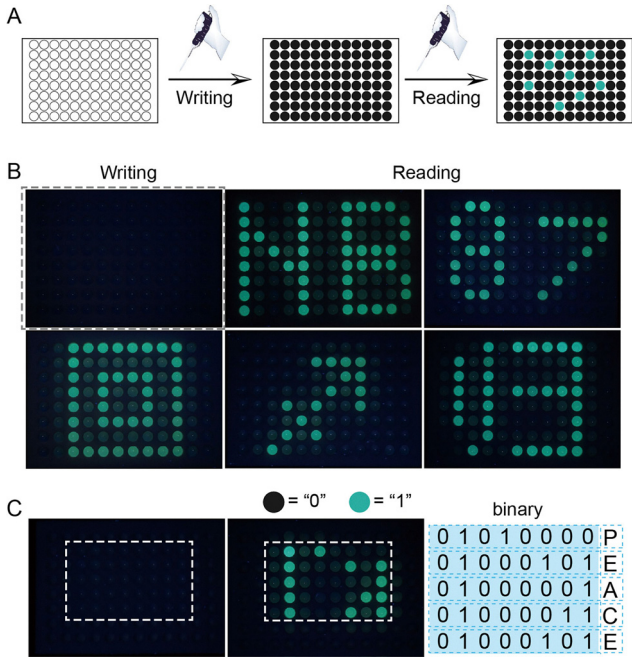

Fig. 5 (A) A schematic diagram of the "writing" and "reading" process. (B) Encoding scheme of English letters, numbers, images, and Chinese characters. (C) Encoding scheme for storage of data for ASCII characters.

off state as "0" and the fluorescent-on state as "1," integrating this phenomenon with binary encoding. Each ASCII character corresponds to a unique binary code, thereby facilitating information input and reading, as well as information anti-counterfeiting. For instance, within the white dashed area of the 96-well plate, a 5 × 8 array utilizes the m-CPBA DCM solution as a reading agent. Under UV light, the corresponding binary information can be read, with the first row's binary representation being "01010000," which corresponds to the character "P," thus enabling the reading of the information "PEACE". This indicates that there is a conceptual application in fluorescence encoding and decoding.

Conclusions

In conclusion, dithieno[3,2-*b*:2′,3′-*d*]thiophene 4,4-dioxide (DTTO) and its halogen-substituted derivatives were synthesized based on an oxidation strategy to provide robust emission. Obvious redshift could be detected for DTTO derivatives in both adsorption and emission, along with the increase in molecular weight of the halogen due to the electron-donating conjugation effect. Additionally, DTTOs displayed robust deep blue emission in THF and pronounced AEE behavior with the formation of aggregates. Single-crystal data reveal that multiple supramolecular interactions suppress intramolecular motion upon aggregation to improve the emission intensity and strong π–π interactions. Moreover, theoretical investigations indicate that DTTOs possess negligible SOC, which suppresses rapid intersystem crossing in the excited state and results in high quantum yield in the single molecular state. Thus, the strategy of reducing SOC through oxidation presents a novel approach for designing organosulfur luminogens with high quantum yields.

Author contributions

H. Liu designed and synthesized the materials, performed all measurements, and wrote the manuscript. Z. Zhuang analysed the photophysical properties and performed theoretical calculations. Y. Hou, Y. Zhu and R. Xu performed single crystal data and visualization. B. Chen, R. Hu and Z. Zhao provided intellectual input and revised the manuscript. All the authors discussed the project and analysed the results.

Conflicts of interest

There are no conflicts to declare.

Data availability

The data supporting this article are available within the article and ESI.† The crystallographic data for DTTO, DC-DTTO, DB-DTTO and DI-DTTO have been deposited at CCDC with deposition numbers 2378966, 2378911, 2378965 and 2378958, respectively.†

Acknowledgements

This research was funded by the National Natural Science Foundation of China (22205120), YongJiang Talent Introduction Programme and Hunan Provincial Natural Science Foundation (2024RC3206).

Notes and references

1 H. Atek, I. Labbé, L. J. Furtak, I. Chemerynska, S. Fujimoto, D. J. Setton, T. B. Miller, P. Oesch, R. Bezanson, S. H. Price, P. Dayal, A. Zitrin, V. Kokorev, J. R. Weaver, G. Brammer, P. V. Dokkum, C. C. Williams, S. E. Cutler, R. Feldmann, Y. Fudamoto, J. E. Greene, J. Leja, M. V. Maseda, A. Muzzin, R. Pan, C. Papovich, E. J. Nelson, T. Nanayakkara, D. P. Stark, M. Stefanon, K. A. Suess, B. Wang and K. E. Whitaker, *Nature*, 2024, **626**, 975–978.
2 M. S. Dodd, W. Shi, C. Li, Z. H. Zhang, M. Cheng, H. D. Gu, D. S. Hardisty, S. J. Loyd, M. W. Wallace, A. V. Hood, K. Lamothe, B. J. W. Mills, S. W. Poulton and T. W. Lyons, *Nature*, 2023, **618**, 974–980.
3 Y. H. Shen, H. V. Dinh, E. R. Cruz, Z. H. Chen, C. R. Bartman, T. X. Xiao, C. M. Call, R. P. Ryseck, J. Pratas, D. Weilandt, H. Baron, A. Subramanian, Z. Fatma, Z. Y. Wu, S. Dwaraknath, J. I. Hendry, V. G. Tran, L. F. Yang, Y. Yoshikuni, H. M. Zhao, C. D. Maranas, M. Wuehr and J. D. Rabinowitz, *Nat. Chem. Biol.*, 2024, **20**, 1123–1132.
4 L. Lückemeier, T. De Vos, L. Schlichter, C. Gutheil, C. G. Daniliuc and F. Glorius, *J. Am. Chem. Soc.*, 2024, **146**, 5864–5871.

5 V. Bizet, C. M. M. Hendriks and C. Bolm, *Chem. Soc. Rev.*, 2015, **44**, 3378–3390.
6 Y. Aota, T. Kano and K. Maruoka, *Angew. Chem.*, 2019, **58**, 17661–17665.
7 L. Zhu, Y. X. Liu, X. F. Wang, K. Zhang, J. W. Tai, Y. Q. Sun, C. Wang, L. Ding, M. K. Fung and J. Fan, *Chem. Eng. J.*, 2023, **473**, 145449.
8 R. Isci, L. Wan, S. Topal, D. Gunturkun, A. J. Campbell and T. Ozturk, *J. Mater. Chem. C*, 2022, **10**(29), 10719–10727.
9 L. Li, J. Li, L. Guo, Y. Xu, Y. Bi, Y. Pu, P. Zheng, X. K. Chen, Y. Wang and C. Li, *Chem. Sci.*, 2024, **15**(29), 11435–11443.
10 Y. Dai, J. Xu, X. Lei, Q. Y. Meng and J. Qiao, *Adv. Funct. Mater.*, 2024, **35**, 2412780.
11 A. J. Gillett, A. Privitera, R. Dilmurat, A. Karki, D. Qian, A. Pershin, G. Londi, W. K. Myers, J. Lee, J. Yuan, S.-J. Ko, M. K. Riede, F. Gao, G. C. Bazan, A. Rao, T.-Q. Nguyen, D. Beljonne and R. H. Friend, *Nature*, 2021, **597**, 666–671.
12 M. Ghasemi, N. Balar, Z. Peng, H. Hu, Y. Qin, T. Kim, J. J. Rech, M. Bidwell, W. Mask, I. McCulloch, W. You, A. Amassian, C. Risko, B. T. O'Connor and H. Ade, *Nat. Mater.*, 2021, **20**, 525–532.
13 J. Hou, O. Inganäs, R. H. Friend and F. Gao, *Nat. Mater.*, 2018, **17**, 119–128.
14 S. Giannini, L. Di Virgilio, M. Bardini, J. Hausch, J. J. Geuchies, W. Zheng, M. Volpi, J. Elsner, K. Broch, Y. H. Geerts, F. Schreiber, G. Schweicher, H. I. Wang, J. Blumberger, M. Bonn and D. Beljonne, *Nat. Mater.*, 2023, **22**, 1361–1369.
15 M. Li, J. Zheng, X. Wang, R. Yu, Y. Wang, Y. Qiu, X. Cheng, G. Wang, G. Chen, K. Xie and J. Tang, *Nat. Commun.*, 2022, **13**, 4912.
16 X. Chen, Z. Wang, J. Qi, Y. Hu, Y. Huang, S. Sun, Y. Sun, W. Gong, L. Luo, L. Zhang, H. Du, X. Hu, C. Han, J. Li, D. Ji, L. Li and W. Hu, *Nat. Commun.*, 2022, **13**, 1480.
17 Z. He, W. Zhao, J. W. Y. Lam, Q. Peng, H. Ma, G. Liang, Z. Shuai and B. Z. Tang, *Nat. Commun.*, 2017, **8**, 416.
18 S. Tian, H. Ma, X. Wang, A. Lv, H. Shi, Y. Geng, J. Li, F. Liang, Z. M. Su, Z. An and W. Huang, *Angew. Chem., Int. Ed.*, 2019, **58**(20), 6645–6649.
19 J. Ma, Y. Zhou, H. Gao, F. Zhu and G. Liang, *Mater. Chem. Front.*, 2021, **5**(5), 2261–2270.
20 J. Zhang, E. Sharman, L. Yang, J. Jiang and G. Zhang, *J. Phys. Chem. C*, 2018, **122**(45), 25796–25803.
21 M. Zhang, L. Zhao, J. Xie, Q. Zhang, X. Wang, N. Yaqoob, Z. Yin, P. Kaghazchi, S. Zhang, H. Li, C. Zhang, L. Wang, L. Zhang, W. Xu and J. Xing, *Nat. Commun.*, 2021, **12**, 4890.
22 M. M. Desjardins, L. C. Contamin, M. R. Delbecq, M. C. Dartiailh, L. E. Bruhat, T. Cubaynes, J. J. Viennot, F. Mallet, S. Rohart, A. Thiaville, A. Cottet and T. Kontos, *Nat. Mater.*, 2019, **18**, 1060–1064.
23 N. W. Hendrickx, D. P. Franke, A. Sammak, G. Scappucci and M. Veldhorst, *Nature*, 2020, **577**, 487–491.
24 T. Kobayashi, J. Salfi, C. Chua, J. van der Heijden, M. G. House, D. Culcer, W. D. Hutchison, B. C. Johnson, J. C. McCallum, H. Riemann, N. V. Abrosimov, P. Becker, H.-J. Pohl, M. Y. Simmons and S. Rogge, *Nat. Mater.*, 2020, **20**, 38–42.
25 J. X. Lin, Y. H. Zhang, E. Morissette, Z. Wang, S. Liu, D. Rhodes, K. Watanabe, T. Taniguchi, J. Hone and J. I. A. Li, *Science*, 2022, **375**, 437–441.
26 N. H. D. Khang, Y. Ueda and P. N. Hai, *Nat. Mater.*, 2018, **17**, 808–813.
27 B. Rasche, A. Isaeva, M. Ruck, S. Borisenko, V. Zabolotnyy, B. Buechner, K. Koepernik, C. Ortix, M. Richter and J. van den Brink, *Nat. Mater.*, 2013, **12**, 422–425.
28 Q. L. He, T. L. Hughes, N. P. Armitage, Y. Tokura and K. L. Wang, *Nat. Mater.*, 2021, **21**, 15–23.
29 P.-H. Lin, B.-Y. Yang, M.-H. Tsai, P.-C. Chen, K.-F. Huang, H. H. Lin and C. H. Lai, *Nat. Mater.*, 2019, **18**, 335–341.
30 E. Tedesco, F. Della Sala, L. Favaretto, B. Giovanna, D. Albesa-Jove, D. Pisignano, G. Gigli, R. Cingolani and K. D. M. Harris, *J. Am. Chem. Soc.*, 2003, **125**, 12277–12283.
31 B. Giovanna, F. Laura and G. Sotgiu, *Chem. Mater.*, 2001, **13**, 4112–4122.
32 S. Lee, H. Koike, M. Goto, S. Miwa, Y. Suzuki, N. Yamashita, R. Ohshima, E. Shigematsu, Y. Ando and M. Shiraishi, *Nat. Mater.*, 2021, **20**, 1228–1232.
33 J. Jang and J. H. Oh, *Adv. Mater.*, 2003, **15**, 977–980.
34 B. Manna, R. Ghosh and D. K. Palit, *J. Phys. Chem. C*, 2016, **120**, 7299–7312.
35 R. Castañeda, V. N. Khrustalev, A. Fonari, J. L. Bredas, Y. A. Getmanenko and T. V. Timofeeva, *J. Mol. Struct.*, 2015, **1100**, 506–512.
36 K. Carter-Fenk and J. M. Herbert, *Chem. Sci.*, 2020, **11**, 6758–6765.
37 R. Castañeda, V. N. Khrustalev, A. Fonari, J.-L. Bredas, Y. A. Getmanenko and T. V. Timofeeva, *J. Mol. Struct.*, 2015, **1100**, 506–512.
38 X. C. Fan, K. Wang, Y. Z. Shi, Y. C. Cheng, Y. T. Lee, J. Yu, X. K. Chen, C. Adachi and X. H. Zhang, *Nat. Photonics*, 2023, **17**, 280–285.
39 N. J. Turro, V. Ramamurthy and J. C. Scaiano, *Modern Molecular Photochemistry of Organic Molecules*, Viva Books, University Science Books, 2017.

